

Global mapping of storm surges and the assessment of coastal vulnerability

**G. R. Brakenridge, J. P. M. Syvitski,
I. Overeem, S. A. Higgins, A. J. Kettner,
J. A. Stewart-Moore & R. Westerhoff**

Natural Hazards

Journal of the International Society
for the Prevention and Mitigation of
Natural Hazards

ISSN 0921-030X

Nat Hazards

DOI 10.1007/s11069-012-0317-z



Your article is protected by copyright and all rights are held exclusively by Springer Science+Business Media B.V.. This e-offprint is for personal use only and shall not be self-archived in electronic repositories. If you wish to self-archive your work, please use the accepted author's version for posting to your own website or your institution's repository. You may further deposit the accepted author's version on a funder's repository at a funder's request, provided it is not made publicly available until 12 months after publication.

Global mapping of storm surges and the assessment of coastal vulnerability

G. R. Brakenridge · J. P. M. Syvitski · I. Overeem · S. A. Higgins ·
A. J. Kettner · J. A. Stewart-Moore · R. Westerhoff

Received: 11 December 2011 / Accepted: 26 July 2012
© Springer Science+Business Media B.V. 2012

Abstract The measurement and recording of the height and spatial extent reached by coastal storm surges is fundamental to scientific progress in understanding these phenomena. Such information is required for better prediction and for risk assessment. Model-based evaluation of increasing delta vulnerability, for example, cannot be tested without long-term, consistent, and sustained observation of actual events. Also, storm surges occur within the temporal context of tidal variation, which must first be characterized through observation. Present standard approaches for measuring storm surges are not optimum. Thus, tidal gauges provide information at one point, whereas the heights reached by surges vary spatially. Also, post-surge ground surveys are expensive, laborious, and commonly lack comparison to similar data obtained for previous surges or for high tides. The advent of moderate spatial resolution, high temporal resolution remote sensing initiated by the launch of the two NASA MODIS sensors greatly reduces these constraints. For over a decade, daily coverage of most coastal land areas, though restricted by cloud cover, has systematically captured the maximum extents reached by both high tides and by storm surges. Automated water classification algorithms are now transforming the incoming image data into GIS water boundary files, again at daily or near-daily time steps. This paper provides a retrospective view of sample storm surges as mapped via these sensors and describes: (a) the present, MODIS-based surface water surveillance system, (b) the mapping enhancement to be provided by frequent-repeat, wide-swath satellite radar imaging, and (c) the emerging prospects for routine global surveillance of storm surge events. Such will be necessary if long-term trends are to be recognized, characterized, and understood, along coastal zones now being affected by both increasing subsidence and rising sea level.

Keywords Storm surges · Tropical cyclones · Remote sensing · Surge modeling

G. R. Brakenridge (✉) · J. P. M. Syvitski · I. Overeem · S. A. Higgins ·
A. J. Kettner · J. A. Stewart-Moore
CSDMS/INSTAAR, University of Colorado, Boulder, CO, USA
e-mail: robert.brakenridge@Colorado.edu

R. Westerhoff
Deltares, Postbox 85467, 3508 AL Utrecht, The Netherlands

1 Introduction

Storm surges in the coastal zone are measured on an at-a-station basis as the difference between the forecast tide and the water level actually reached. Recording such information together with increasingly accurate coastal topography allows interpolation and extrapolation along topographic contour lines to produce a post-surge map of the event (with an implied assumption of hydraulic connectivity). Commonly, high water marks are employed in post-event surveys, and the importance of such work has led to well-developed methodologies for the acceptance of certain field criteria as indicative of actual surge flow or, instead, storm tide. Data-quality assessments are also made according to standard protocols (Melton et al. 2010). An array of points and heights above a specific datum is the result; these points are used either alone or as the basis for spatially continuous mapping of the landward surge limits. Note that storm tide height can be directly measured relative to the geodetic datum; storm surge height is measured, in contrast, above (slowly varying) predicted tide. Such tidal prediction is available, normally, for only point locations: at tidal gauges.

The change to a birds-eye perspective offered by various forms of remote sensing has long had the potential to greatly complement traditional measurement approaches. For example, aerial photography, immediately following a tropical storm landfall and associated storm surge, and once mosaicked and incorporated into an ortho-photograph, can be used to delineate maximum surge extent. However, surges may occur over long stretches of coastline. This and the need for dedicated flight missions, detailed photo-interpretive work, and ground-truthing, make for a major and expensive project. Such projects have quite often been undertaken in the aftermath of catastrophic events causing major damage, but many less extreme surges have not been mapped at all, and the existing mapped surges also suffer from the lack of contextual information and long-term sampling. Single event maps cannot address how large the mapped event was compared to previous ones or how the inundation pattern is changing over time.

Orbital remote sensing, commencing in earnest in the mid-1970s, offers an improvement: large areas can be imaged within single acquisitions, and digital geocoding and land classification methods have been developed, which simplify and improve the mapping process. However, coverage of events is not predictable: the constellation of sensors includes many with too-long revisit times over particular land areas, ranging from weeks to no coverage at all unless specifically requested. Mapping of high water extent is most accurate immediately after the event, and it is only in the past 12 years that appropriate data for all storm surges has become available.

Since the 1999 launch of the first MODIS (Moderate Resolution Imaging Spectrometer) sensor aboard NASA's Terra ("AM," morning pass) satellite platform, and the 2002 launch of a second MODIS aboard Aqua ("PM," afternoon pass), the above data constraints have been removed. These two sensors operate in "always-on" mode, and with associated, public, free, rapid, data distribution systems. They are providing predictable (except for obscuration by cloud cover) coverage over all portions of the Earth, twice daily, and with unprecedented spectral resolution (36 bands). Somewhat similar coverage was available prior to 1999, through the U.S. AVHRR sensor aboard NOAA polar orbiters, but with maximum spatial resolution of only 1 km. MODIS, in contrast, provides 250 m resolution in two (visible and near infrared) bands, and exceptionally accurate geocoding information, so that image pixel locations are known in reference to a global datum to ± 50 m, 95 % rms (root mean square). One of the two bands, 2, at (841–876 nm) was designed, in part, for water/land discrimination; we make use of this inherent capability here in using MODIS to map storm surges.

The following presents examples of remote sensing results to date, emphasizing MODIS. Next, further work in automated remote sensing is described, including synthetic aperture radar (SAR) that is yielding a public GIS data source for routine mapping of all major storm surge events every year. We consider that such information offers a potential revolution in how surges are measured, mapped, and modeled. When extended forward in time, this new capability should make possible better observation and understanding of long-term trends, in particular, those along critical delta shorelines.

2 Examples of storm surge events in the modis era

2.1 Hurricane Katrina

One of the better-studied storm surges during the MODIS era is that associated with Hurricane Katrina (Melton et al. 2010). Katrina made landfall on August 29, 2005, as a category 3 hurricane. Sustained wind speeds were approximately 200 km/h (Knabb et al. 2005). More than 80 % of the city of New Orleans was flooded due to catastrophic levee failures in the hours immediately after Katrina's Gulf Coast landfall; most of the coastline of the State of Mississippi was severely damaged by the storm surge. The eastern side of the Mississippi River Delta was also severely affected by flooding. A variety of space-based remote sensing techniques were employed to map the surge. Figure 1 presents, for example, flooding along the eastern distal portions of the Mississippi Delta as mapped using three different high spatial resolution sensors immediately after the event. A major (100 km²) area of land became open water, and 5–10 cm of sediment was deposited over large areas of the remaining shoreline (Turner et al. 2006).

Melton et al. (2010) measure the spatial accuracy of three different interpolated storm surge surfaces derived from post-event field reconnaissance data by comparing them to a specific run of the SLOSH (Sea, Lake, and Overland Surge from Hurricanes) surge model. "Average surge heights ranged between three and six meters along the Louisiana and Alabama coasts. The western Mississippi coast experienced storm surge as high as seven to nine meters across a path of about 30 km centered approximately on St. Louis Bay, and covered the western half of Harrison County and the eastern half of Hancock County" (Melton et al. 2010).

The SLOSH model uses hurricane pressure, size, forward speed, track, and winds to predict surge height. For comparison purposes, Melton et al. (2010) select the pre-Katrina SLOSH run associated with landfall as a Saffir-Simpson Category 3 hurricane with a central pressure of 927 mb, maximum sustained winds around 203 km/h and potential storm surge between 4.5 and 6 m above normal tide (Fig. 2c). Three independent mapping efforts are compared with the SLOSH run in their study; these mapping efforts differ in their sampling size, method of selecting survey points, and definition of surge, as follows. One team (FEMA) surveyed 306 locations but used only 231 observation points to create their surge inundation representation; this team (Fig. 2a) removed "points that did not match the general trend of elevations in each point's immediate area," thus potentially excluding high water caused by river flooding or wave run-up. They then developed a "three-dimensional storm surge inundation zone using a second power inverse distance weighting approach" and some additional smoothing algorithms, and overlaid this on digital (bare earth) LIDAR topographic data to produce both a map of surge extent and local depth values. A second team (University of Southern Mississippi) also used field surveys focused on strategic locations close to rivers and bayous, and LIDAR topography

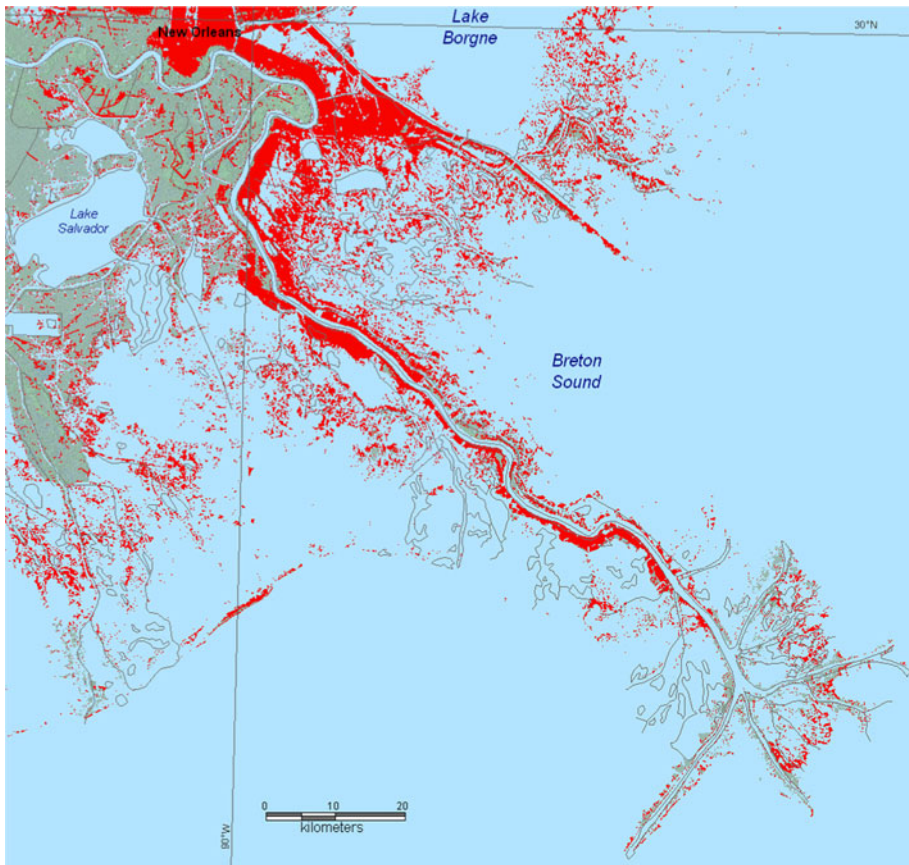


Fig. 1 Inundation (red) of the distal portions of the Mississippi River Delta due to the Hurricane Katrina storm surge, and as mapped by SPOT, RADARSAT, and LANDSAT, August 30 to September 4, 2005. The storm caused 1836 fatalities, many in the city of New Orleans. About 100 km² of wetlands in the Breton Sound Basin were permanently converted to open water

(with 1 m vertical accuracy), but an interpolation strategy that accounts for local obstacles to flow (Fig. 2b). A third university team employed an evenly spaced sampling strategy 6 weeks after landfall, on a 1.6-km grid, and field criteria such as “scour marks, water stains, debris lines and communications from residents.” They employed a “surface representation technique instead of an interpolation approach” and used USGS topographic maps, not LIDAR information (Melton et al. 2010). The authors note that this last method is susceptible to accuracy errors in the topographic information, and that it produced a smaller amount (70 %) of spatial overlap when compared to the first two teams and methods.

Most striking is the exceptional amount of human resources, fieldwork, and high-quality auxiliary data (topographic information) needed in all three efforts to reconstruct water extent and depth, and at considerable time intervals after the event. Meanwhile, orbital remote sensors were repeatedly imaging actual inundation of this landscape as it occurred and then while the landscape was draining (Fig. 2d).

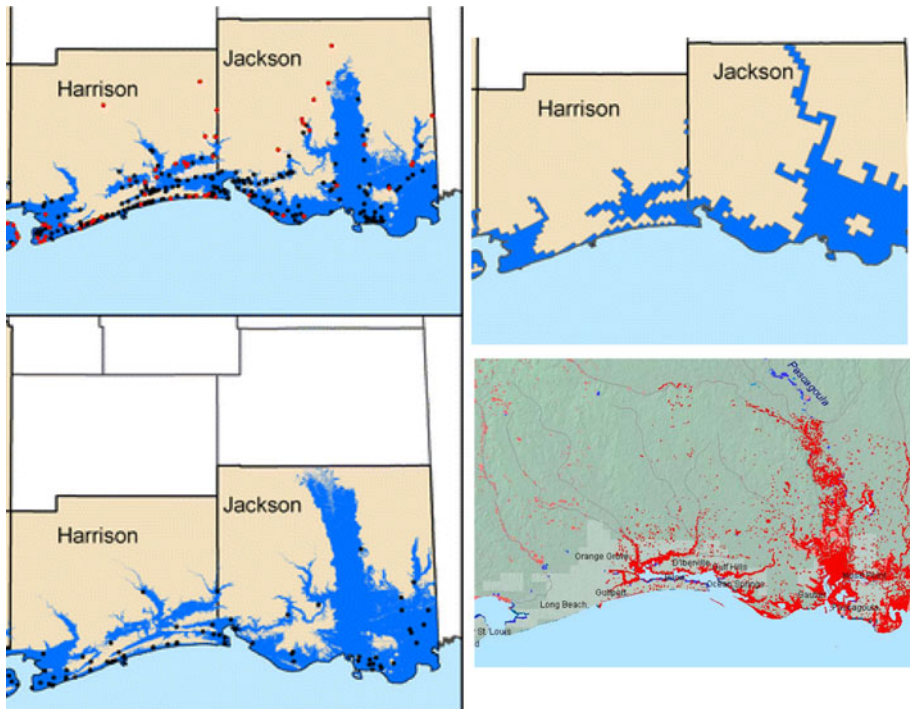


Fig. 2 *Upper left* (FEMA) and *upper right* (University of Southern Mississippi): Post-surge reconstruction of surge extent from field survey, topographic data, and interpolation algorithms. *Lower left* is the storm surge inundation (blue) for Katrina predicted by the SLOSH model. It shows major inundation predicted east of Bay St. Louis (extreme left in figure), north of the Gulfport barrier island (center of the figure), and at the Pascagoula River mouth and extending far upstream (right side of figure). *Lower right* shows inundation as imaged by MODIS on August 30. SLOSH under-predicted surge flooding along the Pascagoula; MODIS did not observe the predicted and observed flooding east of Bay St. Louis. All maps span approximately 620 km east to west; FEMA, University of Southern Mississippi, and SLOSH maps are modified from Melton et al. (2010)

Figure 2 demonstrates the utility of remote sensing in providing further corroboration and crosschecking of varying field results. These two basically different approaches (field versus remote sensing-based) in surge mapping pose an interesting set of contrasting opportunities and constraints: (a) surveys on the ground, within the areas affected, clearly offer the most detailed documentation; (b) such information, however, is obtained from points on a map, and interpolation between points is unavoidable to establish map inundation extent; thus, the final maps still include significant error; (c) remote sensing provides, very economically and immediately, the map view; but (d) remote sensing classification of image elements (pixels) as “surge affected” suffer from classification errors of commission and omission.

One notable error of omission is illustrated in Fig. 2, wherein the MODIS mapping does not show flooding north of Bay St. Louis, whereas the SLOSH model predicted surge inundation there and the post-event surveys document this as well. Examination of the twice-daily MODIS data for this time period indicates that localized cloud cover over this area obscured this part of the surge from observation (Fig. 3). Thus, the MODIS mapping, even when composited over several days, must be utilized as a minimum extent and due to the possibility of cloud obscuration.

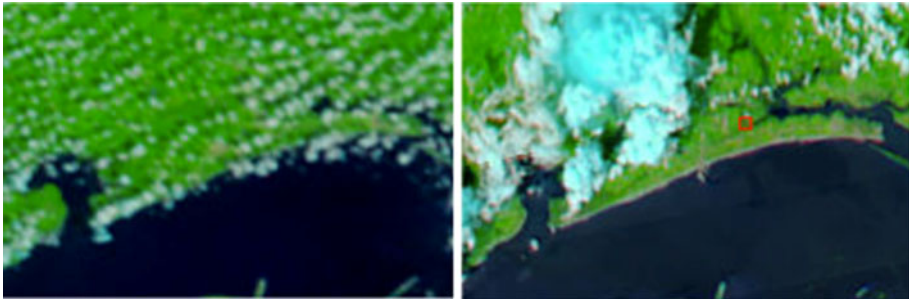


Fig. 3 *Left* image is Terra, morning pass of MODIS, false color (bands 1, 2, and 7), August 26. *Right* image is Aqua, same bands, afternoon pass of MODIS, August 31, 2005 immediately after passage of the storm. Sustained cloud cover over the land area immediately east of Bay St. Louis locally obscured the Katrina storm surge from view. Images span approximately 620 km east–west

Lastly, SLOSH significantly under-predicted the width and extent of the most inland storm surge flooding. This was true especially at vegetated locations within estuaries and upstream along the Pascagoula River (Melton et al. 2010). There are multiple possible causes for under-prediction; these authors indicate that vegetation, buildings, and flow pathways may be inadequately represented in the model and/or the model flow routing algorithm itself may not adequately accommodate them. In either case, despite the vegetation cover (the Pascagoula floodplain is occupied by a mature bottomland forest), remote sensing did accurately observe the landward limits reached by the storm surge (Fig. 2). As illustrated in the next example, this is not always the case along vegetated deltas.

2.2 Cyclone Aila along the Ganges–Brahmaputra Delta

Tropical storms associated with the Indian Monsoon system encounter the Ganges Delta shoreline every few years, and over the last decade, two major hurricanes/cyclones impacted the delta. The Ganges–Brahmaputra delta, extending into Bangladesh and India, is one of the most densely populated deltas in the world, with ~ 150 million inhabitants in 2000 (de Sherbinin et al. 2007; Overeem and Syvitski 2009). Because part of it is forested, accurate remote sensing of storm surge limits can be challenging.

We used Shuttle Radar Topography Mission (SRTM) data to assess low-lying areas in this delta (Syvitski et al. 2009). The vertical precision of SRTM data depends considerably on location, terrain characteristics, and surface feature properties. We employed the SRTM C-band data with a 5.6 cm wavelength, with its near-global relative vertical accuracy of ≈ 3.7 m (Berry et al. 2007), and for many of the world's flat-lying (deltaic) areas an error between 1.1 and 1.6 m (Schumann et al. 2008). Since ocean heights tidally varied over the duration of the mission, a tailored DEM was generated consisting of the static heights over land and tidally adjusted TOPEX/Poseidon-derived ocean heights (Farr et al. 2007). A vector shoreline database (the SRTM Water Body Data Set-SWBD) was employed to depict the ocean coastlines, lake shorelines, and rivers.

SRTM data analysis for the Ganges–Brahmaputra delta shows 1,988 km² of land registers at an elevation below sea level (Fig. 4). Vulnerable low-lying areas rapidly increase in extent when considering that storm surges raise the water level: 6,170 km² are <2 m a.s.l., and 10,770 km² are <3 m a.s.l. (Syvitski et al. 2009). For the Ganges–Brahmaputra, the area estimates based on SRTM data are known to be minimum values: the SRTM data

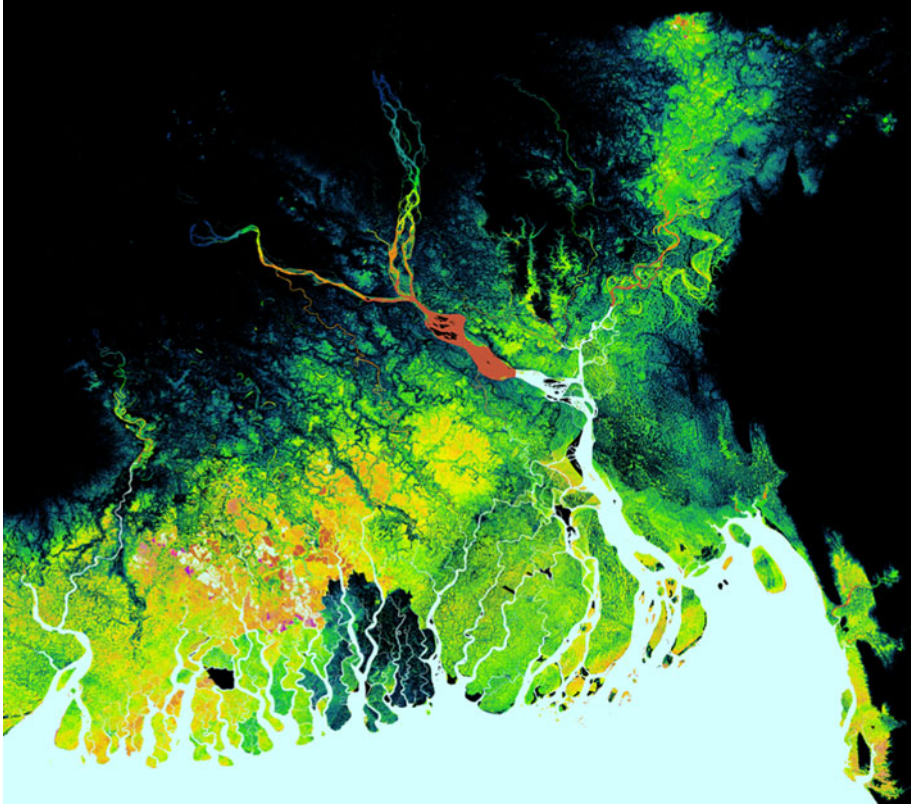


Fig. 4 SRTM topographic data for the Ganges–Brahmaputra delta, with mask above the 10 m a.s.l. elevation contour (from Syvitski et al. 2009). Higher land is shown in red and yellow; green colors are close to sea level; map is 450 km east–west

are derived from C-band radar data, which only partly penetrates canopy. The natural mangrove forests of the Sundarbans in the delta register at 3–6 m height, but they are known to be subjected to flooding at the forest floor almost annually.

Two major hurricanes affected the delta over the MODIS time period; Sidr (November 11–16, 2007), with winds over 250 km/h, classified as a category 4 event on the Saffir–Simpson scale, and Aila (May 24–25, 2009) with winds of 120 km/h categorized as a category 1 event. Aila made landfall near the India–Bangladesh border, and its track passed Kolkata and suburbs, with 14.5 million inhabitants. Early warnings and organized evacuations helped keep fatalities low (330), but at least 1 million people in India and Bangladesh were displaced by the storm as 175,000 homes were destroyed and 270,000 were damaged (Wikipedia 2012). We map here flood extents resulting from merging 8 MODIS images of the coastal zone of the Ganges–Brahmaputra delta after Cyclone Aila.

Figure 5 provides a MODIS optical (bands 1, 2, and 7) georectified color composite image. The flooded areas, especially north of the Sundarbans, are clearly distinguishable. Figure 6 shows mapped results of a water classification algorithm (see last section of this paper) depicting interpreted flooding in the Ganges–Brahmaputra delta resulting from the Aila storm surge. The surge height is estimated at 6.1 m. Red in this map depicts the storm surge inundation mapped by the algorithm; blue areas are water during the February 2002

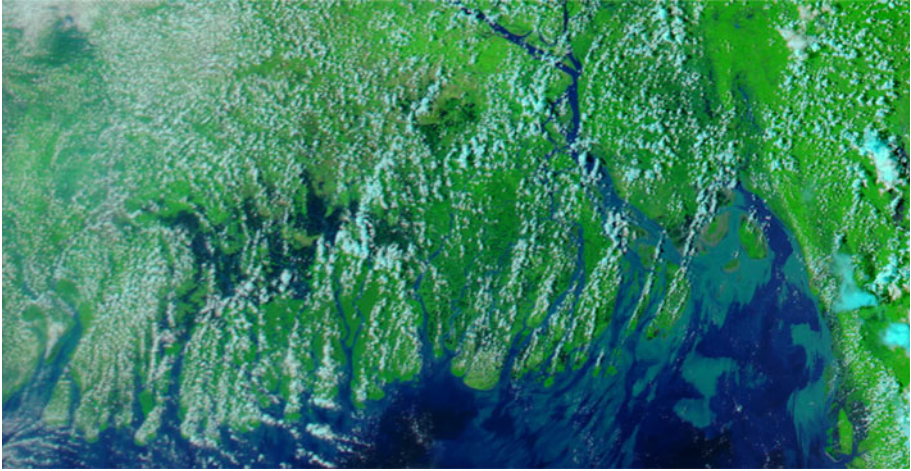


Fig. 5 MODIS view of storm surge flooding inland from Cyclone Aila, May 2009 (*dark blue or black colors*), showing vegetation (mangrove forest) obscuration of flooding closer to the coastline. Data courtesy of NASA MODIS Rapid Response Subsets. Image is 450 km, east–west

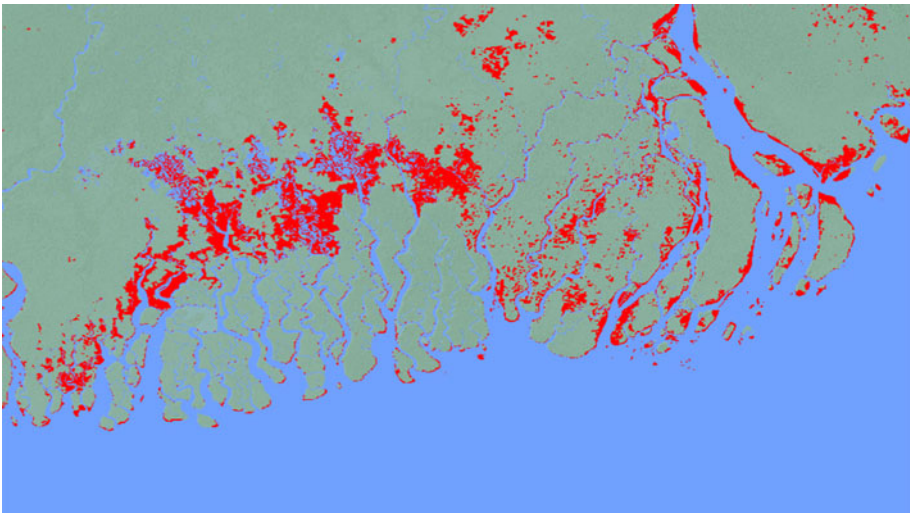


Fig. 6 Overlay of two GIS vector polygon layers created from a total of 8 MODIS images during the aftermath of tropical Cyclone Aila (compare with Fig. 5). *Red* depicts the storm surge flooding from the cyclone and applies to the 4 days after the storm (May 27–30). The reference water layer (*blue*, both marine and freshwater) was created from SWBD-Surface Water Bodies data from SRTM (February, 2000). Layer subtraction shows storm inundation compared to the reference date. Image is 325 km east–west

SRTM mission. In Fig. 6, the coastal fringes are inundated: these areas consist of halophyte and low mangrove vegetation in natural conditions. In the areas outside of the National Park, inhabited areas close to the coastal fringes are protected by ~4- to 5-m high dikes of clay enforced with bricks, and the land directly below is intensely used for rice farming or for shrimp farming. In those areas that were inundated, many of the dikes failed.

In addition, considerable areas north of the Sundarbans forests are flooded; these are mainly agricultural areas including rice paddies. The map does not show flooding that was reported within the Sundarbans National Park. We infer that the dense freshwater swamp forest canopy in this area obscures the flooded forest floor in the MODIS remotely sensed data: this water is hidden from view by this sensor and at these relatively limited spectral bands.

2.3 Surge inundation of Ayeyarwady Delta from Tropical Cyclone Nargis

Nargis was a very strong (category 4) tropical cyclone that caused the worst natural disaster in the recorded history of Myanmar/Burma (Fritz et al. 2009). It made landfall on May 2, 2008 and travelled slowly eastward adjacent to and along the entire delta coastline, causing a strong surge inland of as much as 5 m, above which were waves as high as 2 m. Flooding reached more than 50 km inland (Fig. 7); at least 138,000 fatalities resulted among a population that had previously not experienced such storm events. Several millions were displaced from heavily damaged or destroyed homes; damage estimates were more than \$USD 10 billion. The humanitarian disaster was made worse by the initial unwillingness of the national government to accept international aid. In the days immediately following the event, the MODIS-sourced surge mapping (Fig. 7) provided the only public map information concerning the severity of the event. Such information also provides a valuable constraint to surge modeling.

In this regard, and as for Katrina, post-surge ground survey data (Fritz et al. 2009) have been used in numerical modeling of the surge. The recorded high water marks serve as

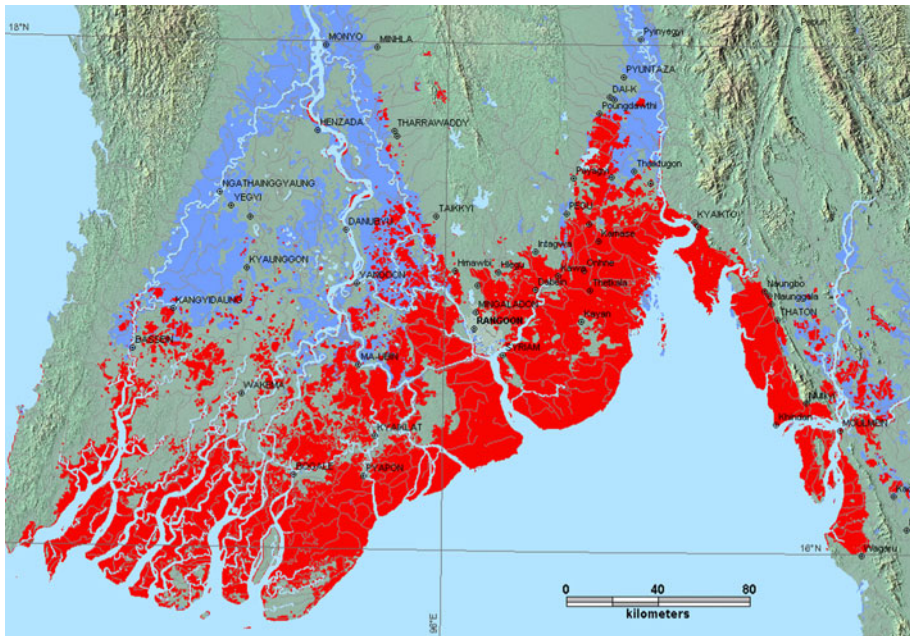


Fig. 7 The intersection of inland and storm surge flooding. *Red* shows May 5, 2008 MODIS mapping of the lethal Tropical Storm Nargis storm surge along the Ayeyarwady Delta and to the east, Myanmar/Burma. The river flooded *blue* areas to the north in prior years. City of Rangoon is at *center* of figure

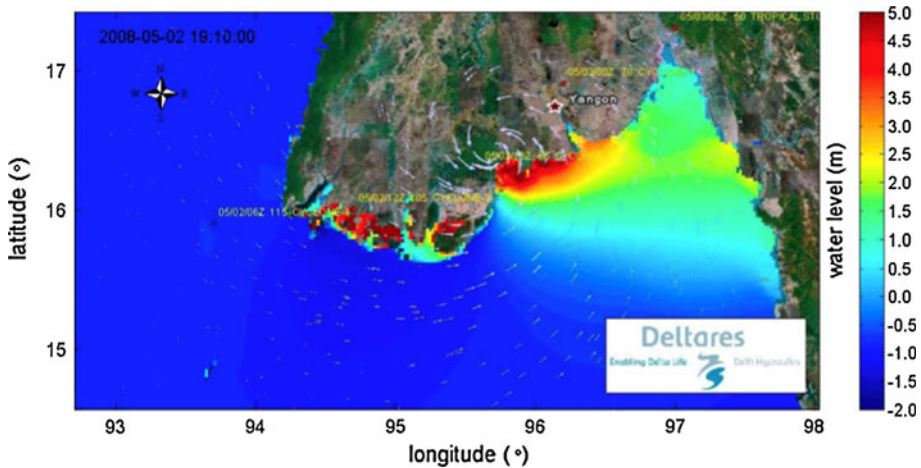


Fig. 8 Numerical modeling of the Nargis storm surge (Deltares 2009). Note modeled +5 m surge south of Rangoon. Compare with Figs. 7 and 9, 10

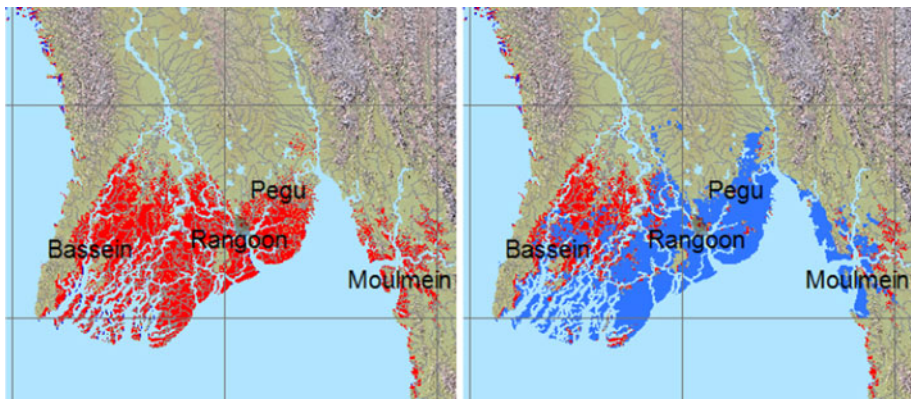


Fig. 9 *Left* image is a shaded relief map of the Ayeyarwady Delta region produced from the NASA SRTM topography. *Red* areas are below 7 m above sea level. *Right* image is MODIS mapping of the Nargis storm surge on May 5, in *blue*

valuable benchmarks for such use, but another approach is to compare remotely imaged inundation to model output. Figure 8 shows calculated water elevation at the moment Cyclone Nargis made landfall and as modeled by the “Delft-Dashboard” modeling tool at Deltares Institute, the Netherlands. As for Katrina, propagation of the surge upstream along inland estuaries is a problem area, apparently due to inadequate topography and bathymetry used in the model (Deltares 2009). Figures 9 and 10 also provide a direct comparison to the NASA SRTM topographic data. The 7 m a.s.l. level contour was chosen to compare the topography to surge inundation. According to Fig. 9, near Pegu, where modeling resulted in the largest surge heights, inundation reached fully 7 m: +2 m above the model prediction. To the east, along gentle shoreward slopes near Moulmein, where the surge limits were also clearly imaged, the remote sensing is in significant disagreement with the model output (Fig. 8). Here, the intersection of water limit with the SRTM

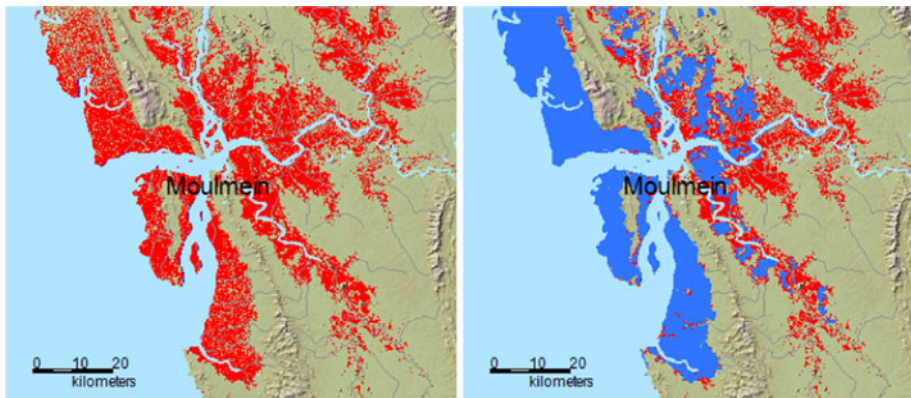


Fig. 10 Detail from the Fig. 9 maps. Sloping shoreline south of Moulmein below the 7 m contour (red area of <math><7\text{ m}</math> topography) closely matches the surge extent (blue area)

topography indicates the water reached 7 m a.s.l. and thus much higher than the predicted 2 m a.s.l.

Possible sources of error in such remote sensing-based surge limit and height determinations include large amounts of freshwater runoff from intense rainfall, and the uncertainty in bareground land surface elevation given the nature of the C-band SAR-based topographic data. Resolution of such discrepancies is outside the scope of this paper. Instead, we stress the clear utility of the remote sensing data for at least two important tasks: (a) providing validation and other constraints needed in order to improve storm surge modeling, and (b), most critically, providing an actual, spatially continuous record of inundation during the surge.

3 Global surveillance of coastal shorelines

Given the value of such post-surge remote sensing, we now consider efforts to make such information widely available, as a routine information resource. In this regard, a prototype global remote sensing daily surface water product has recently become available. Discussion of its components and algorithms, the resulting data product, and the prospects for maintenance and improvements follows. We provide also another example (the 2011 earthquake and tsunami, Japan) that further illustrates the utility of this kind of frequent revisit, wide-area remote sensing when applied to the coastal zone: even when, unlike for deltas, the near-shore topography is steep.

In 2009–2010, a combined NASA/university research group developed the MODIS water algorithm, and NASA is now supporting the ongoing special preprocessing of the MODIS data, which facilitates the production of the automated, near real-time (NRT) global water product. The result includes both daily raster maps (at 10° latitude and longitude increments and 250 m pixel dimensions) and GIS daily water polygons, in.shp format. Public web pages provide access to the map and file results (<http://floodobservatory.colorado.edu/>; <http://oas.gsfc.nasa.gov/floodmap/home.html>).

As noted, this optical data-driven surface water mapping is significantly hindered by cloud cover. Although clear weather immediately after a tropic storm passage is common, most surges occur under storm cloud cover. To address the cloud cover issue, the present

optical processor is currently being joined to a complementary, radar frequency, European Space Agency Envisat ASAR-based surface water processor (Kleuskens et al. 2011; Westerhoff et al. 2010). Both processors will ingest and integrate the other's data output and both can be migrated to similar optical and radar data planned, commencing in 2013 (e.g., the NASA VIIRS sensor, the ESA Sentinel Mission).

At the core of the optical processor is a flexible water classification algorithm that begins by ingesting a 2 day/four image accumulation of MODIS 250 m LANCE-MODIS band 1 and band 2 reflectance data (as reformatted into 10°, Platte Carree projection, Geotiff format mosaics). These mosaics are produced by the NASA LANCE (Land Atmosphere Near Real-time Capability for EOS) processor with <3 h latency from the time of satellite acquisition. The water classification calculates a band 2/band 1 ratio and outputs as "water" all pixels below a constant threshold (using this ratio provides for better scene to scene calibration). Because clouds and cloud shadow on clouds can be recognized by their relatively high reflectance, a built in cloud filter is included: pixels above a specified band 1 reflectance value are excluded regardless of the ratio. The intermediate result is a binary water/land raster for each of the four images.

Unfortunately, surface water and dark cloud shadows cannot, in many cases, be discriminated from each other in single images using only MODIS bands 1 and 2. Incorporating other MODIS bands, at much coarser spatial resolution (500 m and 1 km), would remove the detail appropriate for mapping many surface water changes. Therefore, and making use of the abundant temporal sampling, final pixel classification as water requires 2/4, 3/4, or 4/4 "water" classification results. Most cloud shadows move; the complete algorithm thus makes use of their transient nature to remove them from the final (four image/2 day) classification result. For each following day, the newly updated classification product then makes use of that day's two scenes and those from the day before: this forward-running compositing preserves up-to-date coverage while removing most cloud shadow noise (errors of commission). The final "daily" results (as raster maps and GIS files) are then electronically transmitted to the online access sites. These data can then be used within GIS software to map storm surges, as shown in the results presented here.

The "always-on" capability of the MODIS sensors is thus put to maximum use. Our experience in mapping surface water changes is providing a continuing lesson in this regard: after major disasters, it is this type of sensor and processing methodology that can provide useful data most rapidly. Thus, as noted, MODIS was first to capture the storm surge flooding related to Katrina, in the US Gulf Coast, and from Nargis, in South Asia. More recently, along a long reach of the coastline of Japan, immediately after the 2011 tsunami, MODIS and the automated water product provided a regional survey of the lands affected (Fig. 11).

This event, on March 11, was a magnitude 9.0 megathrust earthquake 70 km off the coast of Japan. It was the most powerful measured earthquake known for Japan and triggered powerful tsunami waves, which reached heights of up to 40.5 m and which in the Sendai area travelled up to 10 km inland. Although great spatial detail along Japan's rugged coastlines was not possible at MODIS resolution, the first MODIS pass, only hours after the tsunami struck, did provide an immediate localization of damaged areas, stretching in a bead-like pattern where rivers enter the sea and along >100 km of coastline (Fig. 11). Thus, the sensor immediately located the location of tsunami run-up, which then allowed high spatial resolution satellites to be immediately tasked to acquire data.

Additional sensors can be integrated into such automated processing schemes to much benefit. One of us (Westerhoff) is part of a team that is further developing the global mode (wide swath, 500 m pixel resolution) of the Envisat ASAR processor (O'Grady et al. 2011)

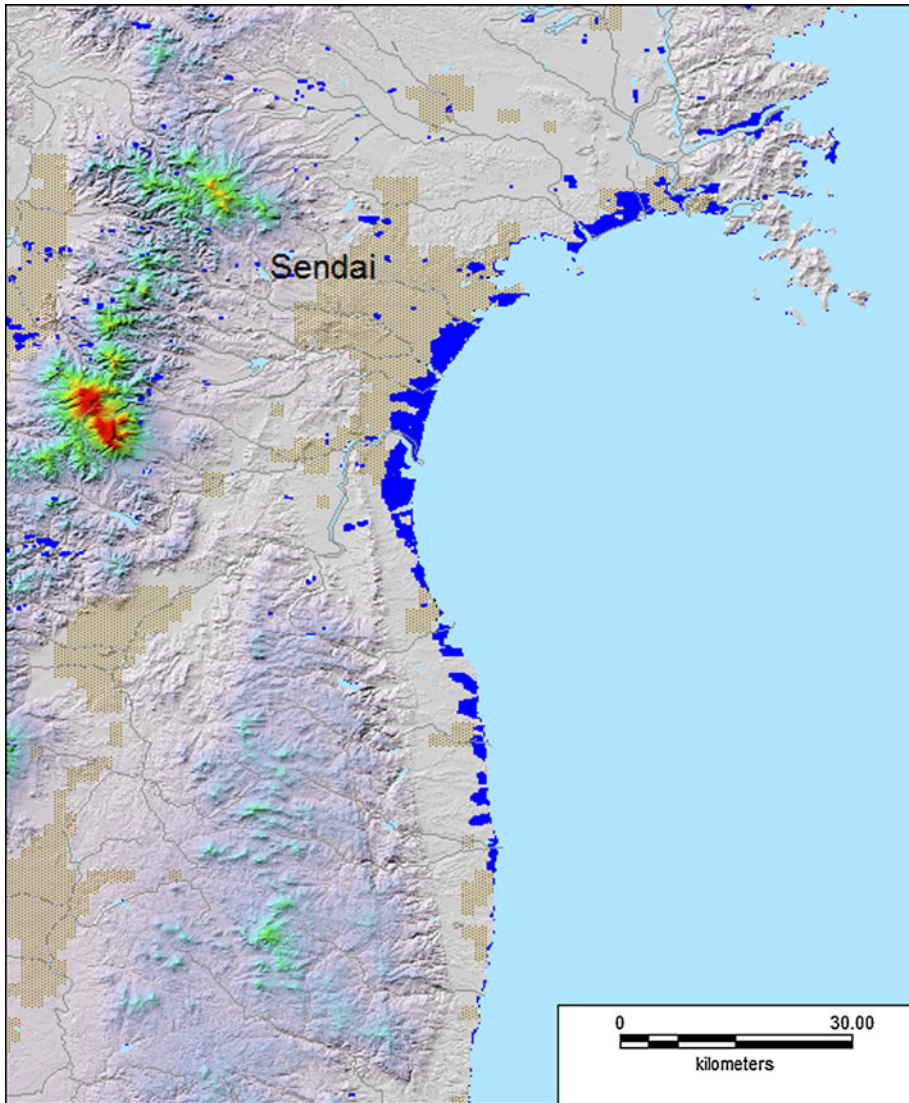


Fig. 11 Landward extent of the 2011 Japanese tsunami, as immediately mapped using the MODIS sensors along this 100-km-long shoreline. This shaded relief map created from SRTM topography. Altitudes range up to 1,500 m above sea level (*red*)

to produce a global flood mapping output. Envisat output in this mode provides near-complete global coverage over approximately 3 days. The prototype system, called “Global Flood Observatory” or GFO, is within a Dutch research programme (Flood Control 2015). The automated system generates global water extent data in near real time and is viewable on Google Earth and/or downloaded as NetCDF files. Level 1 Envisat ASAR data are processed within a maximum of 3 h (but usually much faster) after they appear on a European Space Agency rolling archive. The resulting water product consists

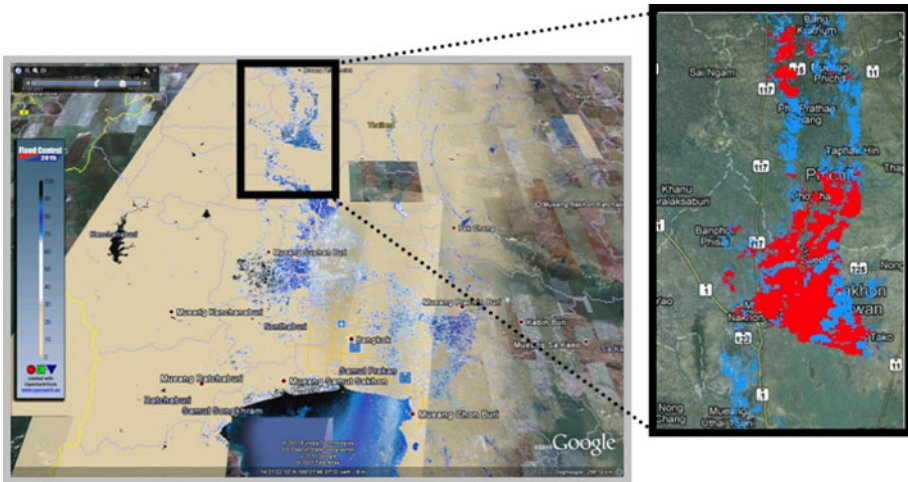


Fig. 12 Merge of MODIS water product (*red*, interrupted by cloud cover) with the Deltares Envisat ASAR water product (*blue*; underneath the *red* layer; display shown on *left*). Discussion is underway toward common map formats, which will show: **a** water mapped via MODIS, **b** water mapped via ASAR, and **c** water mapped by both sensors. The ASAR-based water classification is a probability product (% probability of surface water). In the future, both types of water surveillance technology may be extended via ESA's Sentinel missions, and the U.S. VIIRS and SMAP sensors

of raster files with each pixel including a “water probability” value (0–100 %) and a quality indicator. These data can be used for emergency response in case of storm surge and inland flooding and also for hydrological research and assessments and for assimilation in hydrological modeling (Westerhoff et al. 2010).

The GFO SAR processing methodology data are not hindered by cloud cover; however, it is single wavelength, and reliable water/land discrimination is a challenging task. The processor makes use of the dependence of radar backscatter on radar incidence angle, which varies across the wide swaths used, and the behavior of different land cover types under different viewing geometries. This automated algorithm calculates the probability of a pixel being water by matching its backscatter brightness to a probability distribution of a pre-trained dataset for each 1° longitude \times 0.5° latitude increment of the Earth's surface. This training set includes nearly 3 years of the ASAR Global Mode data. The quality indicator is dependent on backscatter, local incidence angle, and location; it can be used to remove data that are marked as less secure and by calculating water probability only where quality is higher than a threshold, for example, 70 %.

Preliminary tests over ongoing inland flood events indicate that the two systems are producing similar results (Fig. 12). They each include different sources of error, but they are complementary in their effectiveness: the optical data are at higher spatial resolution, but coverage is absent or incomplete during times of heavy cloud cover; the SAR information provides more predictable coverage, but at lower spatial and temporal resolution. Merging the two systems (while preserving capability to operate alone) will provide backup as well as additional automated final data products. Thus, raster (geotiff) flood maps, GIS.shp, and GoogleEarth kml files are or will be generated by both systems, operating in parallel, automatically, and posting their output data on public Web sites.

4 Implications for delta vulnerability assessments

Monitoring surface water variability is important for better defining the global problem of storm surges and subsiding deltas. Many world deltas are supporting local or nearby coastal megacities, such as Dhaka, Bangkok, and Guanzhou. In total, deltas support more than 500 million inhabitants, so the need for regular surveillance to determine the “when and where” of storm surges is evident. This need becomes even more pressing in light of the widespread and rapid subsidence occurring at deltas around the world. In a global survey of 33 representative deltas, 22.5 % had elevations lower than 2 m, and 72,000 km² of these deltas had experienced inundation from one or more coastal surges since the year 2000 (Syvitski et al. 2009). Subsidence at these deltas is driven by both natural and anthropogenic processes, including tectonics, isostasy, global sea level rise (steric effects of ocean volume expansion, ice sheet, and glacier melt contributions), natural substrate compaction, hydrocarbon and water extraction, reduced sediment supply, and human-influenced soil drainage leading to accelerated oxidation (Ericson et al. 2006; Nicholls et al. 2007; Parry et al. 2007).

As a result of these processes, world deltas are sinking at rates 4 times faster, on average, than nearby off-delta areas that better reflect the rise of global sea levels during the twentieth century (Syvitski et al. 2009). If present rates of subsidence on these and other deltas continue, then increasing areas of these and other deltas will likely experience storm surge inundation unless flood defenses are upgraded (Goldenberg et al. 2001; Holland and Webster 2007; Morton et al. 2005). This prediction, however, must be verified by observation in order for mitigation strategies to be effective. In particular, transboundary rivers associated with sinking deltas cannot be effectively managed by one nation alone, and there will be a pressing need for objective river basin information across international borders. Mapping and monitoring by remote sensing can accomplish this goal.

Although modeling studies can be exceptionally valuable for monitoring and predicting storm surge extent, models have associated errors (some are described in this paper). Existing models also represent land subsidence in deltas as a uniform process, applying a single subsidence rate to the entire delta in order to quantify future risk. In reality, land subsidence is highly variable across a delta and through time. Subsidence rates can vary due to the ages of sediment deposits (e.g., Nile Delta, Becker and Sultan 2008), the thicknesses of sediment deposits (e.g., Yellow River Delta, Shi et al. 2007), or even due to differences in the weights of overlying buildings in the Fraser River Delta (Mazzotti et al. 2009). Rates are highest in local areas of rapid groundwater extraction, such as Bangkok or Jakarta (Yong et al. 1995). Oil extraction and mining can also cause rapid short-term subsidence in coastal areas (Finol and Sancevic 1995; Mayuga and Allen 1970). Such activities render digital topographies suspect only a few years after their production; inundation models that rely on them must be updated often. Modeling alone cannot address the need, but instead should be coupled with sustained observation of large and small storm surges as they occur. This observation can further constrain predictive models, which are critical for understanding long-term risk, as well as providing accurate warning of incoming events.

5 Conclusion

Global surveillance of the Earth's changing surface water is now underway. If these remote sensing-based processing systems continue, then the areal extent of land inundation caused

by storm surges, tsunamis, and inland floods will be routinely and systematically observed and recorded in map form. Normal tidal variation along many coastlines, at least locally, exceeds the 250 m MODIS resolution limit: at such locations, sustained observation and mapping now offer the opportunity to fully describe the tidal range in map view instead of at point-site gauges. However, this is new processing technology, and there are known errors of commission (e.g., terrain and cloud shadows misclassified as water) and omission (cloud and vegetation obscuration). More work is needed. The promise of combining both optical and radar wavelength observation of the Earth is bright; they are complementary techniques, and many of the sources of error can be eliminated or reduced. The archived MODIS data extend back to early year 2000, and there is also much potential for backward processing on a daily basis. This would yield a decadal record of the Earth's surface water variability, including surface water caused by storm surges and (within the spatial resolution) global tidal range. As well, satellite-based interferometric monitoring of any ongoing coastal land subsidence can be incorporated (Becker and Sultan 2008).

We have surveyed remote sensing results obtained for three catastrophic storm surges: for Katrina along the U.S. Gulf Coast and Mississippi River delta, for Aila along the Ganges–Brahmaputra Delta in Bangladesh and India, and for Nargis in the Bay of Bengal along the coastline and deltaic lands of Burma/Myanmar. In the first example, and after comparing the results of intensive field surveys as well as SLOSH modeling, we conclude that MODIS remote sensing provided, very economically and immediately, a record of the surge that helps validate predictive modeling and post-event field results. Where the field data indicated some areas of model under-prediction, the remote sensing corroborated such finding. In addition, errors of omission due to cloud cover obscuration were noted in the remote sensing information.

For Aila, the remote sensing surge mapping results delineate many areas of surge inundation, but flooding that was reported within the Sundarbans National Park was not imaged and mapped: we infer that the dense freshwater swamp forest canopy in this area obscured the surge. Perhaps, combination of MODIS optical mapping, SAR-based mapping, and bare-ground topography from LIDAR will be needed to more accurately characterize surges in this region. For Nargis and as for Katrina, comparison of surge modeling to remote sensing indicates that the models under-predict upstream inundation along estuaries. For this event, we also note that the imaged surge limits are in close agreement along some shorelines, but, at some locations, considerably higher-than-modeled heights were reached by the surge: thus pointing to the need for model improvement, and/or better storm tracking/characterization data and land surface information, including topography.

Although the routine surveillance of the Earth's surface, including the coastal zone, at a spatial resolution of 250 m has been ongoing since early year 2000, the utility of such information has been underappreciated until recently. This remote sensing provides only moderate detail, but with very dense sampling in time and with the possibility of automated processing. Automation is made possible, in part, by the space agency investments in precise satellite orbit characterization and the resulting very accurate image geolocation: each successive image of the same region, though without high spatial resolution, can very precisely locate areas of change. We illustrate this for the 2011 Japanese tsunami and also detail how two presently fully automated surface water extent processing systems work, their potential for improvement, and how they can be applied to the coastal zone. Direct applications include the preservation of recent storm surge extents in map form and for future risk assessment, and as sources of data useful for validating and refining predictive storm surge models. The remote sensing capability can also be useful in near real time, immediately after surge-caused disasters, for relief operations and for targeting of higher

resolution sensors, and to gain spatially extensive information about normal tidal and storm wave water variability. If this relatively new-found observational capability can be maintained over years and decades of time, important longer-term issues, such as delta subsidence and vulnerability, can be rigorously addressed, also, by observational data together with models.

Acknowledgments We thank NASA, ESA, and the U.S. National Science Foundation for funding and data support, and also Stichting Deltares and the Flood Control 2015 Project, the Netherlands.

References

- Becker RH, Sultan M (2008) Land subsidence in the Nile Delta: inferences from radar interferometry. *Holocene* 19:949–954
- Berry PAM, Garlick JD, Smith RG (2007) Near-global validation of the SRTM DEM using satellite radar altimetry. *Remote Sens Environ* 106(1):17–27
- de Sherbinin A, Schiller A, Pulsipher A (2007) The vulnerability of global cities to climate hazards. *Environment and Urbanization* 19(1):39–64
- Deltares (2009) Modelling storm surge and flooding during tropical cyclones/hurricanes. Deltares, P.O. Box 177 2600 MH Delft, The Netherlands ZKS-info@deltares.nl <http://www.deltares.nl>
- Ericson JP, Vorosmarty CJ, Dingman SL, Ward LG, Meybeck M (2006) Effective sea-level rise and deltas: causes of change and human dimension implications. *Global Planet Change* 50:63–82
- Farr TG, Rosen PA, Caro E, Crippen R, Duren R, Hensley S, Kobrick M, Paller M, Rodriguez E, Roth L, Seal D, Shaffer S, Shimada J, Umland J, Werner M, Oskin M, Burbank D, Alsdorf D (2007) The shuttle radar topography mission. *Rev Geophys* 45 RG2004. doi:10.1029/2005RG000183
- Finol AS, Sancevic ZA (1995) Subsidence in Venezuela. In: Chillingarian GV, Donaldson EC, Yen TF (eds) *Subsidence due to fluid withdrawal*. Elsevier, New York, pp 337–372
- Fritz HM, Blount CD, Thwin S, Thu MK, Chan N (2009) Cyclone Nargis storm surge in Myanmar. *Nat Geosci* 2:448–449. doi:101038/ngeo558
- Goldenberg SB, Landsea CW, Mestas-Nuñez AM, Gray WM (2001) The recent increase in Atlantic hurricane activity: causes and implications. *Science* 293(5529):474–479. doi:10.1126/science.1060040
- Holland GA, Webster PJ (2007) Heightened tropical cyclone activity in the North Atlantic: natural variability or climate trend? *Phil Trans R Soc* 365:2695–2716
- Kleuskens M, Westerhoff RS, Huizinga J (2011) operational flood mapping: a pilot study in the Mekong area. In: *Proceedings of the international symposium of remote sensing of the environment*, Sydney, Australia, April 10–15 2011
- Knabb RD, Rhome JR, Brown DP (2005) Tropical cyclone report: hurricane Katrina, 23–30 August 2005, (updated 10 August 2006). http://www.nhc.noaa.gov/pdf/TCR-AL122005_Katrina.pdf
- Mayuga MN, Allen DR (1970) Chapter 6, subsidence in the Wilmington Oil Field, Long Beach, California, USA. In: Tison LJ (ed) *Land subsidence*. Int As Sci Hydrol, UNESCO, pp 66–79
- Mazzotti S, Lambert A, der Kooij MV, Mainville A (2009) Impact of anthropogenic subsidence on relative sea-level rise in the Fraser River delta. *Geology* 37(9):771–774
- Melton G, Gail M, Mitchell JT, Cutter SL (2010) Hurricane Katrina storm surge delineation: implications for future storm surge forecasts and warnings. *Nat Hazards* 54:519–536. doi:10.1007/s11069-009-9483-z
- Morton RA, Bernier JC, Barras JA, Ferina NF (2005) Rapid subsidence and historical wetland loss in the Mississippi Delta Plain: likely causes and future implications. US Geological Survey Open-File Report 2005 1216:116
- Nicholls RJ et al (2007) Coastal systems and low-lying areas. In: *Climate change 2007: Impacts, adaptation and vulnerability, contribution of working group II to the fourth assessment report of the intergovernmental panel on climate change*
- O'Grady D, Leblanc M, Gillieson D (2011) Use of ENVISAT ASAR global monitoring mode to complement optical data in the mapping of rapid broad-scale flooding in Pakistan. *Hydrol Earth Syst Sci Discuss* 8. <http://www.hydrol-earth-syst-sci-discuss.net/8/5769/2011/>. doi:10.5194/hessd-8-5769-2011):5769-5809
- Overeem I, Syvitski JPM (2009) Dynamics and vulnerability of delta systems. LOICZ reports and studies, vol 35. GKSS Research Center, Geesthacht, The Netherlands

- Parry ML, Canziani OF, Palutikof JP, van der Linden P, Hanson CE (2007). In: Contribution of working group II to the fourth assessment report of the intergovernmental panel on climate change. Cambridge University Press, UK, pp 315–357
- Schumann GP, Matgen MEJ, Cutler A, Black L, Hoffmann L, Pfister L (2008) Comparison of remotely sensed water stages from LiDAR, topographic contours and SRTM. *J Photogramm Remote Sens* 63:283–296
- Shi C, Zhang D, You L, Li B, Zhang Z, Zhang O (2007) Land subsidence as a result of sediment consolidation in the Yellow River Delta. *J Coastal Res* 23(1):173–191
- Syvitski JPM, Kettner AJ, Overeem I, Hutton EWH, Hannon MT, Brakenridge GR, Day J, Vorosmarty C, Saito Y, Giosan L, R JN (2009) Sinking deltas due to human activities. *Nat Geosc* 2:681–686. doi: [10.1038/ngeo629](https://doi.org/10.1038/ngeo629)
- Turner RE, Baustian JJ, Swenson EM, Spicer JS (2006) Wetland sedimentation from hurricanes Katrina and Rita. *Science* 314:449–452
- Westerhoff RS, Huizinga J, Kleuskens M, Burren R, Casey S (2010) Operational satellite-based flood mapping using the delft-FEWS system. In: Proceedings of the ESA living planet symposium, Bergen, Norway, June 28–July 2, 2010
- Wikipedia (2012) Cyclone Aila. http://en.wikipedia.org/wiki/Cyclone_Aila
- Yong RN, Turcott E, Matthuis H (1995) Groundwater abstraction-induced land subsidence prediction: Bangkok and Jakarta Case Studies. In: Proceedings of the fifth international symposium on land subsidence, IAHS Publ. no 234. The Hague